THE JOURNAL OF PHYSICAL CHEMISTRY C

Article

pubs.acs.org/JPCC

Electrocatalytic Reduction of Oxygen at Single Platinum Nanowires

Stephen J. Percival and Bo Zhang*

Department of Chemistry, University of Washington, Seattle, Washington 98195-1700, United States

Supporting Information

ABSTRACT: Here we report the preparation and electrochemical characterization of single Pt nanowire electrodes with radii ranging from 25 to 130 nm for their electrocatalytic activity toward the oxygen reduction reaction (ORR). Ultralong Pt nanowires were prepared by a laser pulling process. Single Pt nanowire electrodes were fabricated by metal deposition and lithography patterning to expose just a small portion (10−20 μm in length) of the nanowire for electrocatalytic studies. These wires were characterized thoroughly using cyclic voltammetry, under potential deposition of copper, and scanning electron microscopy. We have shown that their electrocatalytic activity toward ORR slightly decreases as the nanowire radius is reduced as measured by the onset potential. Additionally, the current density for the ORR decreases and the mass activity increases as the wire becomes smaller. The faradaic current was modeled on single nanowire electrodes, and the current was found to match the experimental value with outer-sphere redox species. However, significant variance was shown between the modeled ORR current and the measured value. The deviation of the ORR current on the wires is likely due to the presence of F^- ions on Pt and the increased adsorption energy of oxygenated species, thus leading to a hindering of the reaction kinetics of the catalytic process. This is confirmed by Tafel plots where the slope is seen to change at a lower potential as compared to bulk polycrystalline Pt.

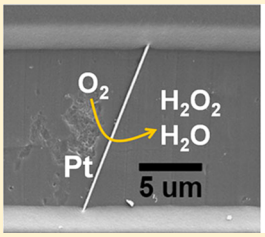

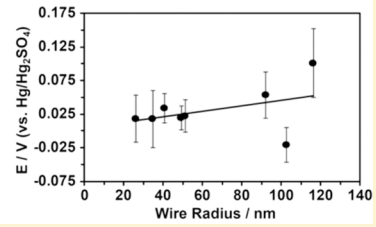

INTRODUCTION

Platinum nanomaterials are widely used electrocatalysts in polymer electrolyte membrane (PEM) fuel cells for the anodic oxidation of a fuel source, such as molecular hydrogen, and are also the catalyst of choice for the cathodic oxygen reduction reaction (ORR).[1] It is well-known that in an acidic electrolyte oxygen can be reduced directly to H_2O through a one-step 4-e^- process or, alternatively, by a two-step 2-e^- process, with H_2O_2 as an intermediate product.[2−4] By reducing the critical dimensions of the electrocatalyst from bulk to nanoscale, the available electrocatalytic surface area per unit mass is greatly increased, allowing more of the reactant to be catalyzed and decreasing the amount of catalytic material.[5]

The majority of previous investigations have utilized large amounts of nanomaterials immobilized on a macroscopic electrode or built into a working fuel cell. As a result, the evaluated performance of such nanomaterial electrocatalysts represents an average of the ensemble.[6] However, the ensemble properties can depend on the spatial organization and particle density of the nanomaterials to one another, affecting the mass transport of reactant and skewing the recorded activities of the nanomaterial.[7] Previous reports speculate the decreasing specific activity (SA) of Pt nanomaterials results from either competition of neighboring catalyst particles for reactant[7] or an increase in adsorption energy for oxygenated chemical species,[8] which slows the ORR kinetics.

To obtain a more complete picture of how the activity and kinetics change with the materials size or composition, studies on single nanowires and nanoparticles become increasingly important. Recently, major advancement has been made using surface plasmon resonance (SPR) to indirectly monitor the reactivity of single Pt nanoparticles.[9] However, minimal investigation has been done in the single nanoparticle or nanowire area where a direct electrical contact is made to the specific nanostructure in question. Recent studies have examined single gold nanoparticles attached to nanoelectrodes[6] or a carbon film[10] and single nanoparticles electrochemically grown on a nanoelectrode.[4,11,12] In addition, nanoelectrodes have been made using single carbon nanotubes,[13,14] and lithographically patterned, electrochemically grown gold nanowires have been used to study electrooxidation at the single nanowire level.[15]

Here we report the fabrication and electrocatalytic study of single Pt nanowire electrodes with radii from 25 to 130 nm toward the ORR. To the best of our knowledge, this is the first reported system where single Pt nanowire electrodes of systematically varying radii have been used to examine an electrocatalytic reaction, such as the ORR. The Pt nanowires were fabricated by mechanically pulling a 25 μm Pt microwire with a laser puller, reducing it to nanoscale and patterning individual nanowires using both photolithography and non-lithographic techniques resulting in a small section (10−20 μm in length) of the wire exposed for testing. These nanowire electrodes were characterized using cyclic voltammetry (CV), copper under potential deposition (UPD), and scanning electron microscopy (SEM). The UPD process was used to

Received: January 13, 2013
Revised: May 23, 2013
Published: June 17, 2013

Scheme 1. Fabrication Steps Used To Contact and Expose the Sides of Single Pt Nanowires for the Study of the ORR

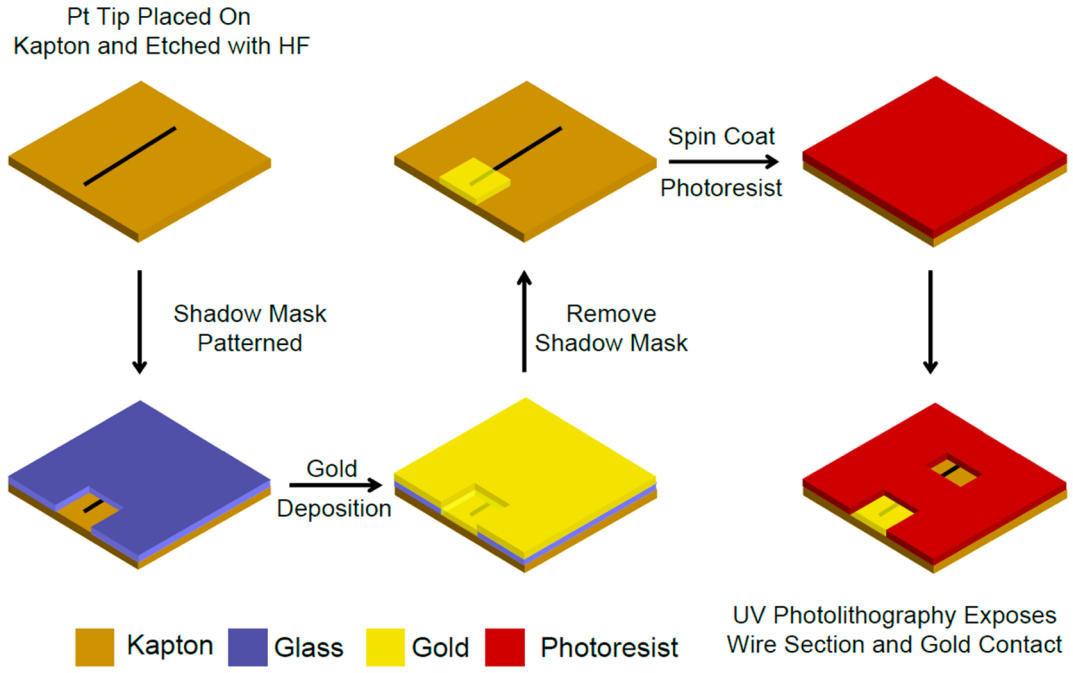

determine the roughness factor for the Pt wires, which can be relevant to the SA for the ORR on the wires. We found that as the wire radius decreases the onset potential shifts negatively and the mass activity (MA) increases while the current density decreases. In addition, we conclude that as the radius of the wire decreases the surface adsorption energy of oxygenated species increases, leading to a decrease in the ORR kinetics at the single Pt nanowires.

EXPERIMENTAL METHODS

Chemicals and Materials. All aqueous solutions were prepared using deionized water (>18 MΩ cm) prepared on a Barnstead Nanopure water purification system. Ferrocene–methanol (FcMeOH, Aldrich, 97%), sodium sulfate anhydrous (Na_2SO_4, J. T. Baker), potassium chloride (KCl, Mallinckrodt Baker), potassium ferricyanide ($K_3Fe(CN)_6$, Sigma-Aldrich 99%), potassium ferrocyanide ($K_4Fe(CN)_6{\cdot}3H_2O$, Fluka, 99.5%), sulfuric acid (H_2SO_4, Fisher), photoresist AZ1512 with AZ351 developer (AZ Corporation, developer diluted 1:5 developer:DI H_2O), hydrofluoric acid (HF, 48 wt % conc, Sigma-Aldrich), sodium fluoride (NaF, J. T. Baker), nitrogen (N_2, >99%, Praxair), oxygen (O_2, >99%, Praxair), and Pt microwire (99.95%, Alfa Aesar, 25 μm diameter) were all used as received from the manufacturers.

Physical Vapor Deposition (PVD). Au pellets (99.999% high purity, Kurt J. Lesker) were placed in tungsten metal evaporation boats and used in the metal evaporator along with chromium-coated tungsten rods (99.999% high purity, Kurt J. Lesker) for deposition of Au/Cr electrodes using an in-house two source PVD system.

Cyclic Voltammetry. Steady-state voltammograms were recorded using a computer-controlled Dagan Chem-Clamp voltammeter/amperometer, and data were recorded using an in-house virtual instrumentation program written in LabView (National instruments) on a desktop PC equipped with a PCI-6251 (National Instruments) data acquisition card. A commercially available Ag/AgCl reference electrode (Bioanalytical Sciences, Inc.) or a Hg/Hg_2SO_4 reference electrode (CH Instruments, Inc.) was used as reference electrode for all CV's, and data were manually baseline corrected and slope corrected. Redox CV's that used KCl salt as the supporting electrolyte were recorded after the ORR experiments in order to prevent contamination from the chloride ion on the Pt surface as it is known to hinder the ORR.[16] The Hg/Hg_2SO_4 reference electrode was used for all ORR studies to prevent chloride contamination to the solution, and all potentials presented are referenced to a Hg/Hg_2SO_4 reference electrode unless otherwise noted. Solutions used for ORR were bubbled with oxygen or nitrogen for >20 min prior to use to ensure the solution was saturated with the desired gas.

Scanning Electron Microscopy. Scanning electron microscope (SEM) images obtained using a field-emission microscope (FEI Sirion) equipped with a through lens secondary electron detector with a resolution of 1–3 nm at the Nanotech User Facility located at the University of Washington. All samples were sputter coated with a 2–3 nm thin conducting layer of Au/Pd prior to SEM imaging.

RESULTS AND DISCUSSION

Fabrication of Single Pt Nanowire Electrodes. The Pt microwires were first mechanically pulled using a CO_2 laser puller according to a method described in detail elsewhere.[17−19] Briefly, a 25 μm diameter Pt microwire was placed in a quartz capillary tube (o.d. 1 mm, i.d. 0.4 mm; Sutter Instrument Co.) and one end sealed closed in a hydrogen/oxygen flame. The quartz capillary was then placed in a P-2000 laser puller (Pull parameters: Heat = 750, Fil = 2, Vel = 60, Del = 140, Pul = 250; Sutter Instrument Co.) and vacuum applied to the unsealed end of the capillary. The laser was first used to heat the quartz around the Pt without pulling the capillary to obtain a tight seal between the quartz and the Pt wire. Once the Pt wire was sealed in the quartz, it was pulled, resulting in two ultrasharp quartz tips with the Pt nanowires sealed inside. This laser

dx.doi.org/10.1021/jp400407n | J. Phys. Chem. C 2013, 117, 13928−13935

method can produce single Pt nanowires with radii as small as 1 nm.

The Pt/quartz tips were broken off and placed on a small square of Kapton (polyimide) film as shown in Scheme 1 and then chemically etched using concentrated HF resulting in a single long (typically >5 mm) tapered nanowire sitting on the Kapton sheet. Gold contact pads (100 nm thick gold film) were thermally evaporated onto the large back end of the nanowire using a simple shadow mask to ensure the gold coated only the desired area. Photoresist (AZ1512) was spin-coated onto the wires and patterned using a chromium-on-glass UV mask to open a small rectangular window (10 × 100 μm) where only the side of the wire would be exposed. This resulted in a hemicylindrical section of the side of the nanowire being exposed from the photoresist, discussed further in the Supporting Information. Resulting lengths of the exposed wires were dependent on whether or not the wire crossed the open window in a straight line perpendicular to the 100 μm edge, and deviation from this ideal configuration resulted in a longer section of exposed wire. Attempts were made to keep the wire lengths equal, but some variability occurred.

SEM and Electrochemical Characterization. The Pt nanowire electrodes were characterized using basic electrochemical methods including cyclic voltammetry with various redox molecules, copper UPD, and SEM. An SEM image of a typical nanowire electrode is shown in Figure 1. The wire is on

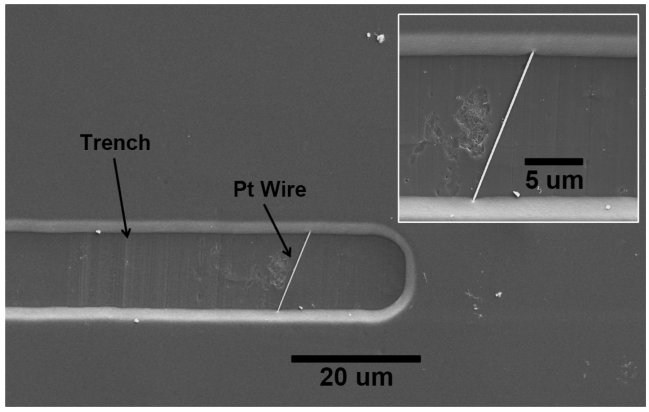

Figure 1. SEM image of a Pt nanowire electrode showing the photoresist trench and a 13.32 μm length of a 92.5 nm radius wire. Inset shows a magnified image of the same nanowire segment.

the Kapton surface and spans the width of the trench. It is important to note that the exposed short nanowire segment in the trench can essentially be viewed as a cylindrical nanowire electrode. Using the SEM images, accurate measurements of the wire dimensions could be made. The radius of a given wire was taken as the average of multiple measurements along the exposed segment of the wire within the trench.

The Pt nanowire electrodes were characterized in various redox solutions including FcMeOH, $K_3Fe(CN)_6$, and $K_4Fe(CN)_6$. Figure 2 shows some characteristic CVs for two nanowire electrodes. Figures 2A and 2B show the CVs for the oxidation of 2 mM FcMeOH on a 19.84 μm long, 40.5 nm radius nanowire and a 20.35 μm long, 116 nm radius nanowire, respectively. The steady-state diffusion-limited current, from these graphs, for the 40.5 nm radius electrode is 1.22 nA and 1.45 nA for the 116 nm radius electrode, both current values taken at 450 mV in the anodic scan direction. More CV's from the same 116 nm radius electrode are shown in Figure 2C for the reduction of 5 mM $K_3Fe(CN)_6$ and in Figure 2D for the oxidation of 5 mM $K_4Fe(CN)_6$. The currents obtained from these CV graphs are 4.43 nA (at −100 mV in the cathodic scan direction) for $K_3Fe(CN)_6$ and 3.41 nA (at 600 mV in the anodic scan direction) for $K_4Fe(CN)_6$.

The steady-state limiting current for a single nanowire can be approximated using the quasi-steady-state equation for a cylindrical shape ultramicroelectrode:[20,21]

$$i_{qss} = \frac{2nFADC}{r \ln(\tau)} \quad (1)$$

Using 1/2 of the area of the cylinder, approximating the wire as a pseudo-hemicylinder further discussed in the Supporting Information, where $A = 2\pi rh$ with r as the radius and h as the length of the cylinder, the i_{qss} effectively becomes equivalent to eq 2, which is that of a hemicylinder[21−23]

$$i_{qss} = \frac{2\pi nFhDC}{\ln(\tau)} \quad (2)$$

where n is the number of transferred electrons per redox molecule, F is Faraday's constant, and D and C are the diffusion coefficient of the redox molecule and its bulk concentration, respectively. A good approximation can be made for τ, being $\tau = (4Dt/r^2)$,[22,24] and the time component, t, can be approximated as $t = (RT/F\nu)$,[25] where ν is the potential scan rate. The approximation shown above gives current predictions that are close to the observed experimental values on the nanowire electrodes.

Using the diffusion coefficient of FcMeOH (6.7×10^{-6} cm^2/s)[26] at 0.050 V/s scan rate with the length and radius for the wire shown in Figure 2A (19.84 μm length and 40.5 nm radius), the limiting current calculated, based on eq 2, is 1.18 nA. This matches very well with the measured limiting current of 1.23 nA. For the wire dimensions used to obtain the CVs in Figure 2B (20.35 μm length with 116 nm radius) the estimated limiting current is 1.44 nA in FcMeOH at 0.050 V/s, which is in excellent agreement with the experimental value of 1.45 nA. To further validate this approximation, the limiting currents were calculated for the electrode in Figure 2B using 5 mM $K_3Fe(CN)_6$ ($D = 7.6 \times 10^{-6}$ cm^2/s)[27] and 5 mM $K_4Fe(CN)_6$ ($D = 6.3 \times 10^{-6}$ cm^2/s),[27] which gave currents of 4.02 and 3.39 nA, respectively. These values again are in close agreement with the measured values of 4.43 and 3.41 nA. These results show that the approximations used to calculate the quasi-steady-state limiting currents can be used to understand the electrochemical response of these nanowire electrodes.

To further characterize these Pt nanowire electrodes, the surface roughness was determined using copper UPD.[28] Surface roughness is related to the geometric surface area, A_g, by a ratio termed the roughness factor, ρ, where $\rho = A_m/A_g$ and A_m is the microscopic or actual surface area. The actual surface area is always larger than the geometric surface area due to crystal grain step edges and microscopic surface texture. To determine the roughness factor, the wires were held for various times at a potential that is more positive than the reversible Nernstian potential for bulk copper deposition so that a monolayer of copper adatoms would be adsorbed onto the Pt surface.[29,30] Once a full monolayer of copper adatoms has formed, no more atoms will deposit onto the surface; the charge obtained from stripping them off is used to calculate the surface area.[31]

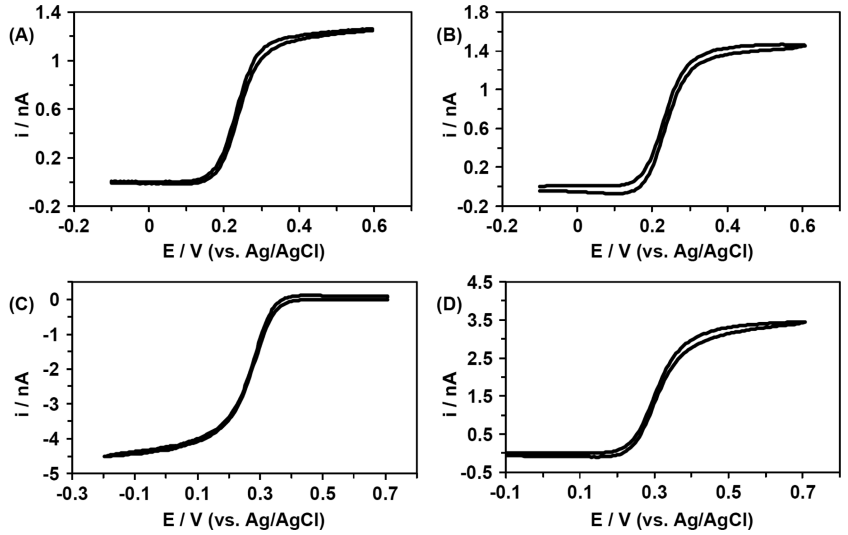

Figure 2. CV's in 2 mM FcMeOH in 100 mM KCl from (A) of a 40.5 nm radius 19.84 μm long Pt nanowire and (B) of a 116 nm radius 20.35 μm long Pt nanowire. (C) and (D) show the CV's from the same wire segment in (B), using (C) 5 mM $K_3Fe(CN)_6$ with 1.5 M KCl and (D) 5 mM $K_4Fe(CN)_6$ with 1.5 M KCl. All scan rates were 50 mV/s.

Figure 3A shows the linear sweep voltammograms from a wire with a length of 21.94 μm and a radius of 49 nm for each

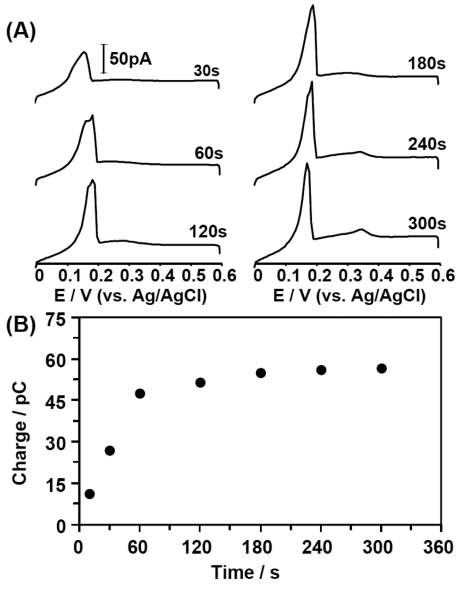

Figure 3. (A) Linear sweep voltammetric responses of a 49 nm radius 21.94 μm long Pt nanowire after copper UPD for different amount of time. The wire was held at 0 V (vs Ag/AgCl) for the amount of time indicated above each trace before initiating the linear sweep; scan rate was 100 mV/s, scale bar is 50 pA. (B) Total charge obtained by integrating the area under the copper stripping peaks shown in (A).

different holding time. The potential was held at 0.0 V (vs Ag/AgCl) in a solution containing 10 mM $CuSO_4$ and 0.5 M H_2SO_4 and then scanned up to 600 mV to strip off the adsorbed copper and the area under the peak integrated to yield the charge. Figure 3B shows the charge graphed as a function of the holding time and shows the amount of charge begins to quickly plateau. By 120 s of holding time the charge changes little with increased holding times. Using the charge of stripping a monolayer of copper off of polycrystalline Pt (410 $\mu C/cm^2$)[32] with an average value of 55.9 pC for the copper stripping charge, a surface roughness of 4.03 was obtained (using the area for the half cylinder). This value is greater than the usual roughness factors reported in the literature, which is likely due to partial exposure of the bottom half Pt surfaces.

Oxygen Reduction Reaction. The main goal of this work was to study electrocatalytic ORR on single Pt nanowires of varying radii. Figure 4A shows a typical CV from a single 116

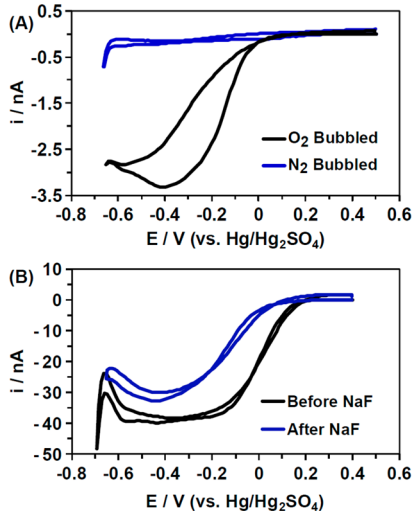

Figure 4. (A) CVs of a 116 nm radius 20.35 μm long Pt nanowire electrode in O_2 bubbled or N_2 bubbled 0.5 M H_2SO_4 and (B) a 12.5 μm radius Pt disk microelectrode in 0.5 M H_2SO_4 bubbled with O_2 showing the effects of a 20 min soak in 200 mM NaF solution on the ORR. All scan rates were 100 mV/s.

nm radius Pt nanowire in N_2-saturated and O_2-saturated 0.5 M H_2SO_4. Figure 4A displays a clear difference in the current responses confirming that the reduction wave in the oxygenated solution is due to reduction of oxygen. Interestingly, the O_2-saturated CV on the nanowire electrode shows a clear hysteresis in the return scan which is significantly greater than that of the Pt disk microelectrode, shown in Figure 4B. This large hysteresis may be an indication that adsorbed fluoride ions on these nanowires interacts somewhat differently

dx.doi.org/10.1021/jp400407n | J. Phys. Chem. C 2013, 117, 13928−13935

(more strongly) with hydrogen, making it more inhibiting for the ORR. The peak current obtained from this wire segment for ORR is 3.31 nA with an onset potential of 101 ± 51 mV. All the onset potentials were taken as 5% of the maximum current observed from the ORR CVs and are the average of the ORR CVs from a single nanowire with the error representing one standard deviation of the average. Conversely, Figure 4B displays the ORR response of a glass-sealed 12.5 μm radius Pt disk electrode in oxygenated 0.5 M H_2SO_4 solution before and after treating in a NaF solution. Here, the NaF treating was used to approximate the nanowires exposure to HF during fabrication. The Pt disk electrode reveals a nice sigmoidal shape voltammetric response, characteristic of enhanced radial-type mass transport at micro- and nanostructures. The reduction of oxygen on the Pt disk happens at an onset potential of 140 ± 8 mV vs Hg/Hg_2SO_4, indicating higher electrocatalytic activity than that demonstrated by the nanowires. The decrease of the reduction current at approximately −0.6 V is likely due to hydrogen adsorption on Pt, which decreases the electrocatalytic activity of the electrode, followed by a sharp increase in current due to proton reduction.

Compared to the inlaid disk, the Pt nanowire electrode shows lower electrocatalytic activity with a negative shift in the onset potential of nearly 39 ± 52 mV for the nanowire with the largest radius. Additionally, starting at around −0.4 V and proceeding until the H^+ reduction potential,[20] the hydrogen adsorption region begins to interfere with the ORR due to adsorbed H^+ ions competing with O_2 for surface sites, leading to a decrease in the reduction current. The decrease in the electrocatalytic activity and the increased competition from the hydrogen region contribute to a somewhat peak-shaped reduction wave as seen in the Figure 4A. These two effects are believed to be due to the contamination of F^- on the Pt surface and are also seen when the potential is started below −0.6 V and scanned positively, as seen in the Supporting Information. The increased competition from adsorbed hydrogen seen on the fluoride contaminated electrode might be due to a large number of platinum surface sites being already blocked by the F^- ions leading to a decrease in available sites for hydrogen adsorption. As a consequence, the overall current is seen to start decreasing at a more positive potential, ∼200 mV, relative to the uncontaminated electrode. The adsorption of F^- is an unexpected consequence of the fabrication process used to etch and release the nanowires from quartz using HF acid. It is well-known that halides such as chloride[16] and bromide[33] are inhibitors of the ORR on Pt by strong surface adsorption and blocking the active catalytic sites and recently fluoride has also been implicated in the poisoning of ORR catalytic sites.[34] However, the Pt disk microelectrode was freshly polished and washed prior to ORR testing to ensure a clean contaminant-free Pt surface.

In order to confirm the inhibiting effect of the F^-, the disk microelectrode was immersed in a 200 mM NaF solution for 20 min and then washed with DI water before ORR testing. A drastic change in the voltammetric behavior of the disk microelectrode before and after NaF soaking is clearly seen in Figure 4B. The CV response of NaF-soaked Pt now becomes more peak shaped much like it is with the nanowire ORR CVs. Additionally, the onset potential is shifted negatively and, in fact, is in the range of measured onset potential for the nanowires. On average, the onset potential for the ORR on the NaF-soaked Pt disk is 73 ± 28 mV as compared to 140 ± 8 mV for the cleanly polished Pt disk electrode. The adsorbed fluoride ion clearly depresses the ORR on the Pt disk and results in an average loss of peak current of ∼8 nA and a negative shift for the onset potential of 67 ± 29 mV. Electrochemical cycling in sulfuric acid (−0.63 to +0.9 V vs $Hg/HgSO_4$) was used to attempt to clean the Pt nanowire electrodes, as it was found to be able to eventually clean and restore the behavior of the Pt disk microelectrode. We believe the sulfuric acid cycling started to cause dissolution of the nanowires and evidence can be seen in SEM images included in the Supporting Information. Despite this, the nanowires were cycled for a limited time to clean them, but cycling was kept to a minimum so as not to significantly etch the nanowire.

The results of all the ORR testing on nanowires with various radii are presented in Figure 5, which shows the onset potential

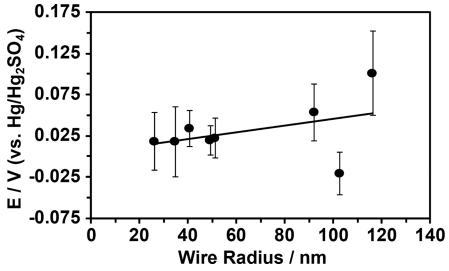

Figure 5. Relationship between the onset potential and the wire radius for the ORR for each nanowire, taken as 5% of the maximum current observed for each CV. Error bars indicate one standard deviation from the mean onset potential for each individual nanowire.

as a function of the wire radius. As seen from this graph, as the radius of the wire decreases, the onset potential shifts slightly to more negative potentials, indicating relatively lower catalytic activity. The onset potential for the nanowires is lower than that of the Pt microelectrode, being at ∼140 mV; however, it does come close for the largest nanowire with an onset potential of 101 mV as discussed previously. The slight negative shift of the onset potential with decreasing nanowire size shows a weak dependence in the activation energy barrier for the ORR on the nanowires radius. It is likely that the more negative onset potentials on single nanowires compared to the large Pt disk is mainly due to F^- adsorption. This may also partially account for the loss in electrocatalytic activity of conventional fuel cell electrode catalysts. During regular operation in a fuel cell, especially at higher temperatures and/or for periods of extended operation, the catalyst layer may be exposed to fluoride ions due to partial decomposition of fluorinated proton exchange membranes (such as Nafion),[5] in the presence of unreacted hydrogen peroxide[35] or at elevated operating temperatures.[36]

As the electrodes decrease in dimension, the current density is expected to increase due to increased mass transport rates.[4,37] When comparing the Pt nanowires to the Pt disk microelectrode, the current density is larger for FcMeOH on all of the wires. An increase in current density for FcMeOH was observed as the wire radius decreased and exhibited a maximum current density on the 26 nm radius wire as shown in Figure 6A. This wire had a limiting current of 0.524 nA, yielding a current density of 60.2 mA/cm^2. The limiting current for FcMeOH predicted using eq 2 is 0.596 nA, giving a calculated current density of 68.4 mA/cm^2, which is in fair agreement to the experimental values. Interestingly, the current density for ORR decreased as the radius decreased also shown in Figure

dx.doi.org/10.1021/jp400407n | J. Phys. Chem. C 2013, 117, 13928−13935

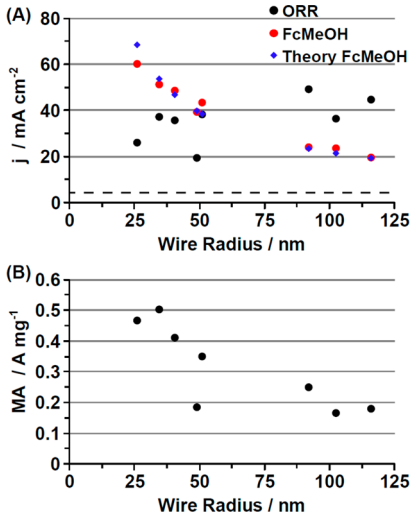

Figure 6. (A) Current density vs wire radius for the 2 mM FcMeOH with the theoretical current density of 2 mM FcMeOH calculated from eq 2 and the current density for the ORR using the geometric surface area; dashed line at ~4 mA/cm^{-2} represents the Pt disk ORR current density. (B) Mass activity for the wires as a function of the wire radii.

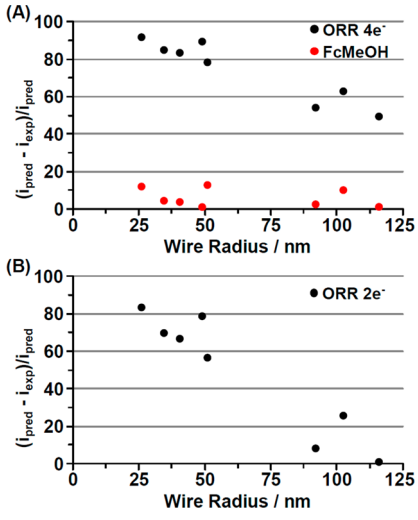

Figure 7. (A) Percent difference between experimental and calculated peak currents for FcMeOH and ORR assuming n = 4 e$^-$ and (B) ORR percent difference assuming n = 2 e$^-$. i_{exp} is the experimentally obtained current, and i_{pred} is the calculated current from eq 2 using 1/2 the area of the cylinder for each wire segment.

6A. The current density for the Pt disk was found to be 4.55 mA/cm^2 for the ORR corresponding to the dashed line in Figure 6A and 1.41 mA/cm^2 for FcMeOH (not shown). All of the nanowires had a higher ORR current density than the Pt disk electrode, despite decreasing as the radius decreased. Figure 6B shows the mass activity for the nanowires increases as the nanowire radius decreases contrary to the current density trend and can be attributed to the increased surface/volume ratio. A similar effect of a decreasing current density and increasing mass activity has been observed before for decreasing Pt particle size.[8,38] This observation was thought to be a result of competition effects for reactant through overlapping spherical diffusion layers between closely spaced nanoparticles.[7] The fact that these are single nanowires further validates reports[8,38] that the decrease in current density is not due to competition between nanoparticle ensembles, although very high nanoparticle loadings can certainly lead to competition.

To further investigate the decreasing current density with wire radius, the predicted currents for the single nanowires, using eq 2, were calculated with the assumption that the number of electrons involved is n = 4 for a complete reduction of oxygen using the O_2 diffusion coefficient, $D = 1.4 \times 10^{-5}$ cm^2/s, and concentration, $C = 1.10 \times 10^{-6}$ mol/cm^3, of oxygen saturated in 0.5 M H_2SO_4 at 25 °C.[39] When the current is calculated for the 12.5 μm radius Pt disk using the equation for a disk microelectrode,[20] a calculated current of 40.2 nA is obtained in excellent agreement to its measured value of 40.9 nA, validating our assumptions for calculating the ORR currents for the single nanowires. Figure 7 shows the percent difference between the experimentally obtained current and the predicted current, for both FcMeOH and ORR. Some difference between currents were expected because FcMeOH is a simple outer-sphere 1-e$^-$ redox species, and its CV is essentially diffusion limited while the oxygen is an inner-sphere species and its reduction involves diffusion, adsorption, catalytic reduction, and desorption of the products. The percent difference for FcMeOH is, at most, ~12% different from experimental results, and for the majority of the wires tested it is below 5% difference. However, for the ORR the percent difference is dramatically intensified to upward of 91.7% for the smallest radius wire, yet just 49.5% for the largest, where the experimental currents obtained were all below the predicted ORR current. This result indicates that the reaction of oxygen on Pt nanowires is far from diffusion limitation.

Chen and Kucernik[4] found that on single electrodeposited Pt nanoparticles, as the size decreases, the effective electron number used in the ORR also decreases, meaning more hydrogen peroxide is formed that would otherwise have been reduced to water. Additionally, on nanoparticles smaller than 50 nm, about 75% of the oxygen is reduced to water and 25% is reduced to hydrogen peroxide.[4] Another factor in the discrepancy between the predicted and experimental ORR currents can be partially explained by the contamination of the fluoride ion. When comparing the calculated 40.2 nA current to the experimental 32.7 nA for the NaF exposed Pt disk electrode, there is a 18.7% difference. The fluoride contamination could be contributing to the decrease in observed current by shifting the reaction mechanism from the 4-e$^-$ reduction more to the 2-e$^-$ reduction, which could be analogous to how adsorbed copper atoms block catalytic sites forcing the oxygen to adsorb in an end-on configuration.[32] The percent difference of the ORR using the assumption n = 2 for the H_2O_2 pathway can be seen in Figure 7B. Even with this extreme assumption, upward of 83% of the predicted ORR current is still not observed for the smallest wire. This indicates the observed experimental current on the nanowires is limited by the kinetics of the ORR and not the diffusion of the molecules to the surface and that more importantly the kinetics slow down as the wire radius decreases. The decrease in current density has been seen in Pt nanoparticle ensembles that vary in diameter and is proposed to be a result of the increasing adsorption energy of oxygenated species.[8,40]

Tafel plots from the ORR for a 26 nm radius wire and the Pt disk microelectrode are shown in Figure 8 and display the characteristic change in Tafel slopes, indicating a change in adsorption from Tempkin isotherm to Langmuir isotherm.[38,41] The high overpotential (low current density) region has a Tafel slope of around 60 mV/decade corresponding to an oxide-

dx.doi.org/10.1021/jp400407n | J. Phys. Chem. C 2013, 117, 13928−13935

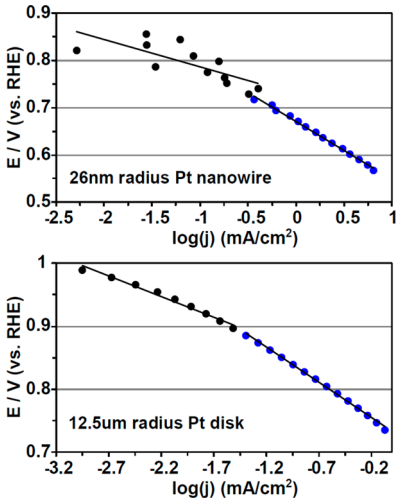

Figure 8. Tafel plots for a 26 nm radius Pt nanowire and a Pt disk microelectrode; scan rates were 100 mV/s. The shift between slopes for the nanowire is seen to happen at a lower potential than the Pt disk.

covered Pt surface. The low overpotential (high current density) region has a slope of ~120 mV/decade corresponding to an oxide-free Pt surface.[41,42] Additionally, the change in the slope on the 26 nm wire occurs at around 0.8 V (vs RHE), whereas the change occurs at 0.9 V (vs RHE) on the polycrystalline Pt disk. The lower potential necessary for the slope change on the nanowire indicates higher adsorption energy for oxygenated species.[8,38,40] Oxygenated species, such as OH^- or HO_2^-, are more strongly adsorbed to the Pt surface hindering the ORR kinetics leading to a decrease in the catalytic activity of the Pt wires for the ORR.[40]

CONCLUSIONS

In conclusion, electrodes were made from single Pt nanowires that were mechanically prepared with a laser pulling method in order to study the catalytic ORR on single Pt nanowires of decreasing radii. The electrocatalytic activity has been found to be dependent on the nanowire size revealed from a change of the onset potential. A clear increase in the mass activity is observed as the wire radius is decreased. It was found that the nanowires were contaminated with fluoride ions that inhibit the ORR, possibly resulting in a decreasing density of catalytic sites as the wire narrows, which may help account for the notable decrease in ORR current density of the nanowires. The Tafel plots indicate increased adsorption energy of oxygenated species to the Pt nanowire surface due to the switching of the Tafel slopes at a lower potential for the wires than for the polycrystalline Pt. This increase in the adsorption strength slows the ORR kinetics and lowers the observed current density. The decreases in the ORR experimental current, with respect to the calculated current, is seen to be a combination of both fluoride anion adsorption to catalytic sites blocking the ORR and a decrease in the ORR kinetics from the higher adsorption energy of oxygenated species.

Future nanowires used for catalytic reaction studies will be etched out of the quartz coating using hydroxide which will eliminate the contamination from the fluoride ions and allow a more detailed understanding of these Pt nanowires. Additionally, catalytic studies using single nanowires in organic, alkaline, and acidic solutions are possible using a photodefinable polyimide that once patterned and cross-linked will be able to withstand harsh chemical environments. Despite the hurdles, these wires hold a unique opportunity to study a range of phenomena where single nanowires offer a versatile platform to more fully understand the changing properties of bulk materials at nanoscale dimensions.

ASSOCIATED CONTENT

Supporting Information

A schematic of the Pt nanowire electrode showing the platinum wire and photoresist beneath it, resulting in blockage of the bottom half of the nanowire from the redox solution, an additional SEM image showing the electrochemically cycled nanowire electrode, and an ORR CV scan of the Pt disk electrode in acidic media where the potential is started at a negative potential and scanned positively. This material is available free of charge via the Internet at http://pubs.acs.org.

AUTHOR INFORMATION

Corresponding Author

*E-mail zhang@chem.washington.edu; phone (206) 543 1767.

Notes

The authors declare no competing financial interest.

ACKNOWLEDGMENTS

The authors gratefully acknowledge the financial support from the Defense Threat Reduction Agency (DTRA) (Contract HDTRA1-11-1-0005). Part of this work was conducted at the University of Washington NanoTech User Facility, a member of the National Science Foundation, National Nanotechnology Infrastructure Network (NNIN), and the Washington Technology Center (WTC).

REFERENCES

(1) Du, S. Pt-Based Nanowires as Electrocatalysts in Proton Exchange Fuel Cells. *Int. J. Low-Carbon Technol.* **2012**, *7*, 44−54.
(2) Markovic, N. M.; Schmidt, T. J.; Stamenković, V.; Ross, P. N. Oxygen Reduction Reaction on Pt and Pt Bimetallic Surfaces: A Selective Review. *Fuel Cells* **2001**, *1*, 105−116.
(3) Gewirth, A. A.; Thorum, M. S. Electroreduction of Dioxygen for Fuel-Cell Applications: Materials and Challenges. *Inorg. Chem.* **2010**, *49*, 3557−3566.
(4) Chen, S.; Kucernak, A. Electrocatalysis Under Conditions of High Mass Transport Rate: Oxygen Reduction on Single Submicrometer-Sized Pt Particles Supported on Carbon. *J. Phys. Chem. B* **2004**, *108*, 3262−3276.
(5) Borup, R.; Meyers, J.; Pivovar, B.; Kim, Y. S.; Mukundan, R.; Garland, N.; Myers, D.; Wilson, M.; Garzon, F.; Wood, D.; et al. Scientific Aspects of Polymer Electrolyte Fuel Cell Durability and Degradation. *Chem. Rev.* **2007**, *107*, 3904−3951.
(6) Li, Y.; Cox, J. T.; Zhang, B. Electrochemical Responses and Electrocatalysis at Single Au Nanoparticles. *J. Am. Chem. Soc.* **2010**, *132*, 3047−3054.
(7) Watanabe, M.; Sei, H.; Stonehart, P. The Influence of Platinum Crystallite Size on the Electroreduction of Oxygen. *J. Electroanal. Chem.* **1989**, *261*, 375−387.
(8) Kabbabi, A.; Gloaguen, F.; Andolfatto, F.; Durand, R. Particle Size Effect for Oxygen Reduction and Methanol Oxidation on Pt/C inside a Proton Exchange Membrane. *J. Electroanal. Chem.* **1994**, *373*, 251−254.
(9) Shan, X.; Díez-Pérez, I.; Wang, L.; Wiktor, P.; Gu, Y.; Zhang, L.; Wang, W.; Lu, J.; Wang, S.; Gong, Q.; Li, J.; Tao, N. Imaging the Electrocatalytic Activity of Single Nanoparticles. *Nat. Nanotechnol.* **2012**, *7*, 668−672.

(10) Kleijn, S. E. F.; Lai, S. C. S.; Miller, T. S.; Yanson, A. I.; Koper, M. T. M.; Unwin, P. R. Landing and Catalytic Characterization of Individual Nanoparticles on Electrode Surfaces. *J. Am. Chem. Soc.* **2012**, *134*, 18558−18561.
(11) Velmurugan, J.; Noel, J.-M.; Nogala, W.; Mirkin, M. V. Nucleation and Growth of Metal on Nanoelectrodes. *Chem. Sci.* **2012**, *3*, 3307−3314.
(12) Sun, P.; Li, F.; Yang, C.; Sun, T.; Kady, I.; Hunt, B.; Zhuang, J. Formation of a Single Gold Nanoparticle on a Nanometer-Sized Electrode and Its Electrochemical Behaviors. *J. Phys. Chem. C* **2013**, *117*, 6120−6125.
(13) Heller, I.; Kong, J.; Heering, H. A.; Williams, K. A.; Lemay, S. G.; Dekker, C. Individual Single-Walled Carbon Nanotubes as Nanoelectrode for Electrochemistry. *Nano Lett.* **2005**, *5*, 137−142.
(14) Campbell, J. K.; Sun, L.; Crooks, R. M. Electrochemistry Using Single Carbon Nanotubes. *J. Am. Chem. Soc.* **1999**, *121*, 3779−3780.
(15) Xiang, C.; Güell, A. G.; Brown, M. A.; Kim, J. Y.; Hemminger, J. C.; Penner, R. M. Coupled Electrooxidation and Electrical Conduction in a Single Gold Nanowire. *Nano Lett.* **2008**, *8*, 3017−3022.
(16) Stamenkovic, V.; Markovic, N. M.; Ross, P. N., Jr. Structure-Relationships in Electrocatalysis Oxygen Reduction and Hydrogen Oxidation Reactions on Pt(111) and Pt(100) in Solutions Containing Chloride Ions. *J. Electroanal. Chem.* **2001**, *500*, 44−51.
(17) Shao, Y.; Mirkin, M. V.; Fish, G.; Kokotov, S.; Palanker, D.; Lewis, A. Nanometer-Sized Electrochemical Sensors. *Anal. Chem.* **1997**, *69*, 1627−1634.
(18) Li, Y.; Bergman, D.; Zhang, B. Preparation and Electrochemical Response of 1−3 nm Pt Disk Electrodes. *Anal. Chem.* **2009**, *81*, 5496−5502.
(19) Katemann, B. B.; Schuhmann, W. Fabrication and Characterization of Needle-Type Pt-Disk Nanoelectrodes. *Electroanalysis* **2002**, *14*, 22−28.
(20) Bard, A. J.; Faulkner, L. R. *Elecrochemical Methods*, 2nd ed.; John Wiley & Sons: New York, 2001.
(21) Kovach, P. M.; Caudill, W. L.; Peters, D. G.; Wightman, R. M. Faradaic Electrochemistry at Microcylinder, Band and Tubular Band Electrodes. *J. Electroanal. Chem.* **1985**, *185*, 285−295.
(22) Morris, R. B.; Franta, D. J.; White, H. S. Electrochemistry at Pt Band Electrodes of Width Approaching Molecular Dimensions. Breakdown of Transport Equations at Very Small Electrodes. *J. Phys. Chem.* **1987**, *91*, 3559−3564.
(23) Wehmeyer, K. R.; Deakin, M. R.; Wightman, R. M. Electroanalytical Properties of Band Electrodes of Submicrometer Width. *Anal. Chem.* **1985**, *57*, 1913−1916.
(24) Szabo, A.; Cope, D. K.; Tallman, D. E.; Kovach, P. M.; Wightman, R. M. Chronoamperometric Current at Hemicylinder and Band Microelectrodes: Theory and Experiment. *J. Electroanal. Chem.* **1987**, *217*, 417−423.
(25) Lanyon, Y. H.; Arrigan, D. W. M. Recessed Nanoband Electrodes Fabricated by Focused Ion Beam Milling. *Sens. Actuators, B* **2007**, *121*, 341−347.
(26) Anicet, N.; Bourdillon, C.; Demaille, C.; Moiroux, J.; Savéant, J.-M. Electron Transfer in Organized Assemblies of Biomolecules. Step-by-Step Avidin/Biotin Construction and Dynamic Characteristics of a Spatially Ordered Multilayer Enzyme Electrode. *J. Electroanal. Chem.* **1996**, *410*, 199−202.
(27) Von Stackelberg, M.; Pilgram, M.; Toome, W. Bestimmung Von Diffusionskoeffizienten Einiger Ionen in Wassriger Losung in Gegenwart Von Fremdelektrolyten 1. *Z. Elecktrochem.* **1953**, *57*, 342.
(28) Zhan, D.; Velmurugan, J.; Mirkin, M. V. Adsorption/Desorption of Hydrogen on Pt Nanoelectrodes: Evidence of Surface Diffusion and Spillover. *J. Am. Chem. Soc.* **2009**, *131*, 14756−14760.
(29) Leiva, E. Recent Developments in the Theory of Metal UPD. *Electrochim. Acta* **1996**, *41*, 2185−2206.
(30) Tindall, G. W.; Cadle, S. H.; Bruckenstein, S. Inhibition of the Reduction of Oxygen at a Platinum Electrode by the Deposition of a Monolayer of Copper at Underpotential. *J. Am. Chem. Soc.* **1969**, *91*, 2119−2120.
(31) Elliott, J. M.; Birkin, P. R.; Bartlett, P. N.; Attard, G. S. Platinum Microelectrodes with Unique High Surface Areas. *Langmuir* **1999**, *15*, 7411−7415.
(32) Machado, S. A. S.; Tanaka, A. A.; Gonzalez, E. R. Underpotential Deposition of Copper and Its Influence in the Oxygen Reduction on Platinum. *Electrochim. Acta* **1991**, *36*, 1325−1331.
(33) Markovic, N. M.; Gasteiger, H. A.; Grgur, B. N.; Ross, P. N. Oxygen Reduction Reaction on Pt(111): Effects of Bromide. *J. Electroanal. Chem.* **1999**, *467*, 157−163.
(34) Thorum, M. S.; Hankett, J. M.; Gewirth, A. A. Poisoning the Oxygen Reduction Reaction on Carbon-Supported Fe and Cu electrocatalysts: Evidence for Metal-Centered Activity. *J. Phys. Chem. Lett.* **2011**, *2*, 295−298.
(35) Curtin, D. E.; Lousenberg, R. D.; Henry, T. J.; Tangeman, P. C.; Tisack, M. E. Advanced Materials for Improved PEMFC Performance and Life. *J. Power Sources* **2004**, *131*, 41−48.
(36) Lage, L. G.; Delgado, P. G.; Kawano, Y. Thermal Stability and Decomposition of Nafion Membranes with Different Cations Using High-Resolution Thermogravimetry. *J. Therm. Anal. Calorim.* **2004**, *75*, 521−530.
(37) Mirkin, M. V.; Bard, A. J. Simple Analysis of Quasi-Reversible Steady-State Voltammograms. *Anal. Chem.* **1992**, *64*, 2293−2302.
(38) Gamez, A.; Richard, D.; Gallezot, P.; Gloaguen, F.; Faure, R.; Durand, R. Oxygen Reduction on Well-Defined Platinum Nanoparticles Inside Recast Ionomer. *Electrochim. Acta* **1996**, *41*, 307−314.
(39) Gochi-Ponce, Y.; Alonso-Nuñez, G.; Alonso-Vante, N. Synthesis and Electrochemical Characterization of a Novel Platinum Chalcogenide Electrocatalyst with an Enhanced Tolerance to Methanol in the Oxygen Reduction Reaction. *Electrochem. Commun.* **2006**, *8*, 1487−1491.
(40) Antoine, O.; Bultel, Y.; Durand, R. Oxygen Reduction Reaction Kinetics and Mechanism on Platinum Nanoparticles Inside Nafion. *J. Electroanal. Chem.* **2001**, *499*, 85−94.
(41) Damjanovic, A.; Sepa, D. B. An Analysis of the pH Dependence of Enthalpies and Gibbs Energies of Activation for O_2 Reduction at Pt Electrodes in Acid Solutions. *Electrochim. Acta* **1990**, *35*, 1157−1162.
(42) Sepa, D. B.; Vojnovic, M. V.; Vracar, M. L.; Damjanovic, A. Different Views Regarding the Kinetics and Mechanisms of Oxygen Reduction at Pt and Pd Electrodes. *Electrochim. Acta* **1987**, *32*, 129−134.